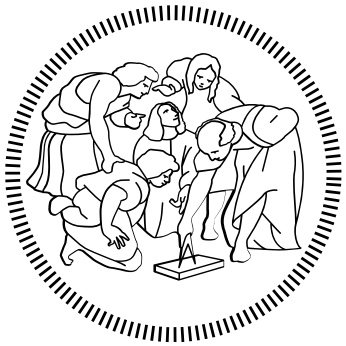

POLITECNICO
MILANO 1863

Modeling of a blow-down propulsion system

Course of Space Propulsion
Academic Year 2023-2024

Lockheed Martini Group

Alessandro Pallotta	alessandro1.pallotta@mail.polimi.it	10712370
Alex Cristian Turcu	alexcristian.turcu@mail.polimi.it	10711624
Chiara Poli	chiara3.poli@mail.polimi.it	10731504
Daniele Paternoster	daniele.paternoster@mail.polimi.it	10836125
Marcello Pareschi	marcello.pareschi@mail.polimi.it	10723712
Paolo Vanelli	paolo.vanelli@mail.polimi.it	10730510
Riccardo Vidari	riccardo.vidari@mail.polimi.it	10711828

Contents

Nomenclature

Acronyms

LRE	Liquid Rocket Engine
LOX	Liquid Oxygen
RP-1	RP-1 fuel
AM	Additive Manufacturing

Symbols

a	[m/s]	Speed of sound
A	[m^2]	Area
B	[-]	Blow-down ratio
c_P	[J/kg K]	Specific heat at constant pressure
c_T	[-]	Thrust coefficient
c^*	[m/s]	Characteristic velocity
C_d	[-]	Discharge coefficient
D	[m]	Diameter
E	[m/s]	Erosion rate
f	[-]	Darcy friction factor
h	[W/m^2 K]	Convective heat transfer coefficient
H	[m]	Height
i	[-]	First iteration index
I_{sp}	[s]	Specific impulse
I_{tot}	[N s]	Total impulse
j	[-]	Second iteration index
k	[m]	Radius of curvature
K	[-]	Pressure loss coefficient
L	[m]	Length
L^*	[m]	Characteristic length
m	[kg]	Mass
$\dot{m}$	[m/s]	Mass flow rate
M	[-]	Mach number
$\mathbb{M}$	[kg/mol]	Molar mass
N	[-]	Number of
O/F	[-]	Oxidizer to fuel ratio
$\overline{O/F}$	[-]	Mean O/F ratio
p	[Pa]	Pressure
Δp	[Pa]	Pressure loss / difference
Pr	[-]	Prandtl number
$\dot{q}$	[W/m^2]	Heat flux
$\dot{Q}$	[W]	Heat transfer rate
r	[-]	Recovery factor
R	[J/kg K]	Specific gas constant
$\mathcal{R}$	[J/mol K]	Universal gas constant
Re	[-]	Reynolds number
Re'	[-]	Modified Reynolds number
t	[s]	Time
Δt	[s]	Time step
T	[K]	Temperature
$\mathbb{T}$	[N]	Thrust
u	[m/s]	Velocity
V	[m^3]	Volume
ΔV	[m^3]	Volume change
α_{AM}	[deg]	Deposition angle of AM
α_{con}	[deg]	Convergent semi-aperture angle
β	[%]	Injector pressure drop as percentage of initial combustion chamber pressure
γ	[-]	Heat capacity ratio
δ	[deg]	Cone angle of fictitious conical divergent
ε	[-]	Area ratio
θ	[deg]	Angle of Rao parabolic divergent
λ	[-]	Nozzle losses coefficient
μ	[Pa s]	Dynamic viscosity
ρ	[kg/m^3]	Density
σ	[-]	Correction factor across boundary layer

Subscripts

aw	Adiabatic wall
b	Burn
c	Combustion chamber
cea	From CEAM software
con	Convergent
div	Divergent
e	Nozzle exit
eff	Effective
f	Final
fd	Feeding lines
fu	Fuel
i	Initial
id	Ideal
inj	Injector
max	Maximum
min	Minimum
ox	Oxidizer
p	Propellants
pr	Pressurizer gas
r	Real
t	Nozzle throat
tc	Thrust chamber
tk	Tank
tot	Total
wg	Gas side wall

1 Introduction and literature overview

In this work a preliminary design of a 1 kN semi-cryogenic LRE (LOX/RP-1) equipped with a blow-down feeding system is discussed. In particular, a first literature analysis was done in order to review previous studies regarding this particular architecture. Recent developments in additive manufacture (AM) techniques were analyzed to obtain some knowledge regarding processes and precision of this new frontier. Moreover, due the reduced size of this system, some criticalities regarding boundary layer and erosion losses were researched. The second part of the paper aim at designing the engine with some imposed initial conditions and some assumptions. The whole dimensioning of the system, including the tanks and feeding lines, is carried on including the dynamics of the system. The final sizing will accomplish the maximization of the total impulse, with the initial and final constraints. An off-design analysis is then performed to quantify the performances with nozzle losses and AM uncertainties. Finally, a feasibility analysis of nozzle fuel cooling is discussed.

1.1 Blow-down heritage

The blow-down architecture is the simplest feeding technique for LRE since it does not require additional pressurizing gas tanks with failure-prone pressure regulator valves nor complex turbomachinery. The scheme includes only two liquid propellant tanks filled with helium or nitrogen, eventually separated by a membrane. The major downsides of this simplicity is relative to the non-stationarity of the tank pressures that induce chamber pressure drop, decrease of propellant mass flow rate and as a consequence O/F ratio variation. This chain of events degrades performances overtime and must be carefully evaluated since combustion efficiency relies upon viable domains of injection pressure and correct mass flow ratio. The interest on blow-down is although justified with respect to well-known pressure regulated feed system since this last can also manifest some criticalities in terms of long-term reliability. In particular, propulsion systems play crucial roles for mission success, such as long interplanetary trips, and they must ensure failure-free lifetime. This is a major concern when focusing on pressure regulated feeding lines in which a pressure regulator valve is present. This kind of elements can be quite complex and hence add a weakness for the whole system[1]. Considering these facts, a blow-down type architecture could be of interest since it decrease system complexity. Moreover, different feasibility analysis for blow-down units are present in the literature in which also an external re-pressurization tank is considered[2]. This is an upgrade that allows to recover performance of the feeding pressure and hence combustion properties. Although the valve complexity is removed since a pyro valve can be used to discharge the gas with a single shot application, the eventual re-pressurization can be a crucial point as the sudden change in pressure could induce unwanted instabilities. Other configurations could foresee the use of a Venturi valve to maintain constant mass flow rate by cavitating the liquid and choking the flow on the feeding line. However, neither extra tank nor Venturi valves will be considered in this work in order to meet the requirements presented in subsection 2.1.
The whole evaluation of the dynamics of the examined propulsion system was not based upon previous works, instead a self-made model was developed.

1.2 Additive manufacturing state of art

1.3 Analysis of losses

2 Modelling of propulsion system: DRY-1

The workflow for the sizing of DRY-1 is introduced by Figure 1 and it is divided into three stages:

- **Input data**: the problem is set up.
- **Nominal sizing**: the system is sized according to initial conditions and general assumptions.
- **System dynamics**: an iterative process is set up to model the blow-down dynamics and finalize the sizing.

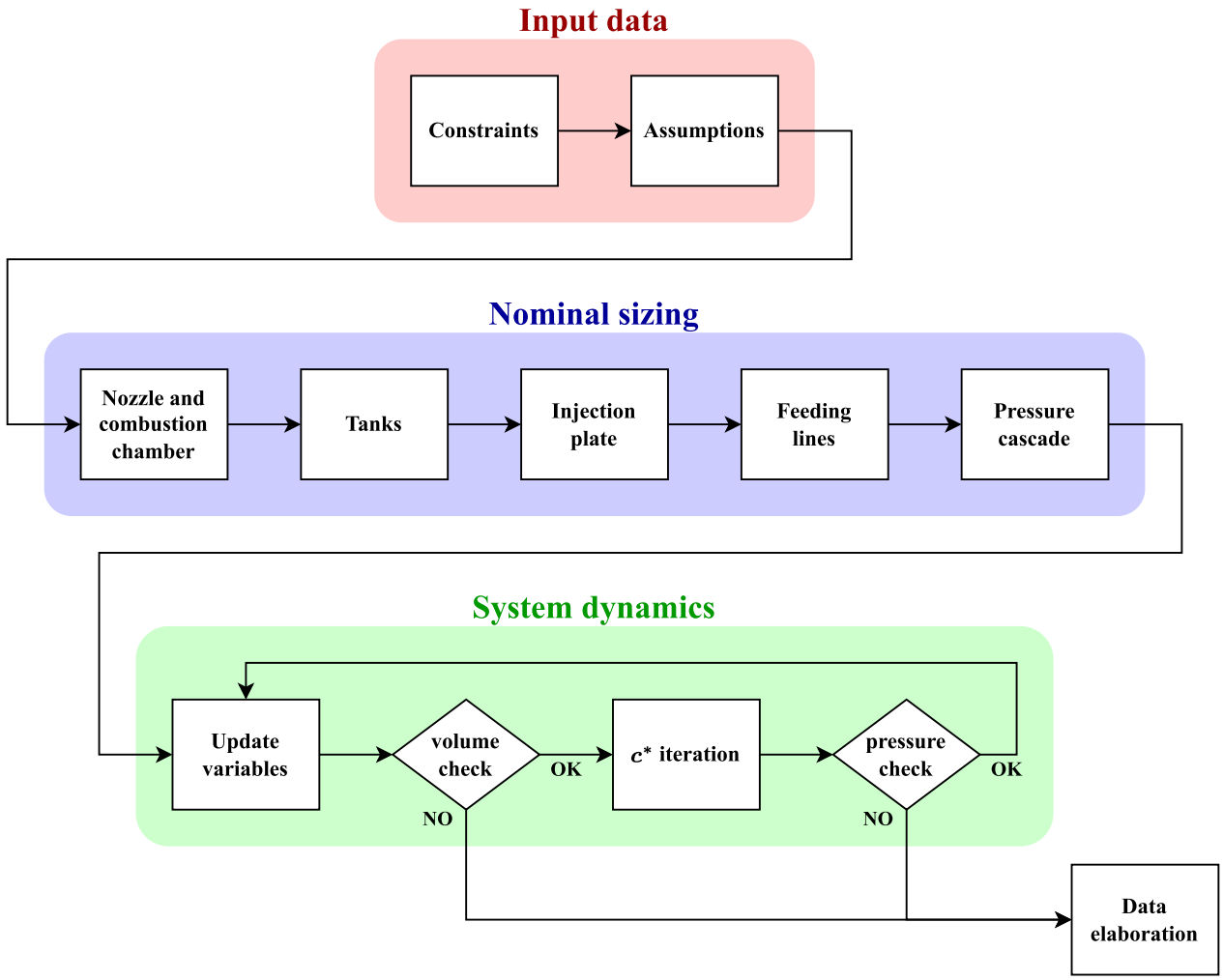

Figure 1: Flowchart of the simulation model

2.1 Input data

The input data defined different kind of requirements, related to operability environment, engine performance, size constraints, chemistry, architecture and manufacturing techniques. Regardless of the development of the engine design, the system shall respect the following pinpoints:

- **Environment**: vacuum for the whole operation.
- **Thrust** $\mathbb{T}$: initial magnitude of 1 kN, no lower boundary.
- **Chamber pressure** p_c: initial value of 50 bar, always above 20 bar throughout the whole mission.
- **Allocated space**: tanks, combustion chamber and convergent nozzle occupancy is exactly 80% of the volume occupied by a cylinder of 1 meter diameter and 2 meter length. No bounds on the extension of the divergent.
- **Propellants**: semi-cryogenic couple of LOX and RP-1.
- **Architecture**: blow-down type.
- **Manufacturing**: all the system is produced in AM, no restriction on material nor techniques.

The nominal sizing refers to the design of the overall system considering the imposed initial constraints as static conditions. This design choice was dictated by the dynamics of the blow-down system, which imposes the maximum flow rate at the beginning of the mission, leading to the oversizing of the engine throughout the rest of the mission.
Various hypothesis were necessary to develop the system, this values are reported in Table 1.

O/F [-]	ε [-]	ε_{con} [-]	L^* [m]	D_{inj}^{fu} [mm]
2.42	300	10	1.143	1

Table 1: Hypothesis from literature and previous design

The choices of L^* and O/F were only dictated by the propellant couple[3], while ε was chosen as the characteristic of the engine refers to an in-space application[4]. Regarding the value of ε_{con} a mean value between 5 and 15 was taken. Smaller values entails longer combustion chamber and small cross sectional area, with large pressure drops. Larger values refers to bigger chamber cross sectional area, with limited length for the combustion. From the literature the suggestion for the choice of this value is to refer to previous successful engines design, considering the same application[5]. Therefore, a 400 N bi-propellant apogee motor was taken as reference and revealed a value of $\varepsilon_{con} \approx 10$[4].

2.2 Nominal sizing

After defining the main input data, the workflow is carried out as shown in Figure 1. All the combustion simulations were performed with Nasa-CEA software, implemented in Matlab (CEAM). In particular the "rocket problem" was considered, Bray model was applied for the expansion (frozen point at the throat), infinite combustion chamber ($M_c = 0$), initial injecting temperatures of the propellant equal to the storage temperatures. The chamber pressure was set as $p_c = 50$ bar and the mixture ratio as $O/F = 2.42$. Latter refinement of this last value will be performed. The output values used from the simulation are represented in table Table 2(vacuum value is considered for the c_T):

c^* [m/s]	c_T [-]	T_c [K]	γ_c [-]
1851	1.935	3708	1.1405

Table 2: First run on CEAM

From this results, the propellant mass flow rate and the throat area can be calculated:

$$\dot{m}_p = \frac{\mathbb{T}}{c_T c^*} \qquad A_t = \frac{\dot{m}_p c^*}{p_c} \tag{1}$$

From the geometry assumption of Table 1, the nozzle exit area and the combustion chamber geometry can be retrieved:

$$A_e = \varepsilon A_t \tag{2}$$

$$A_c = \varepsilon_{con} A_t \qquad L_c = \frac{L^*}{\varepsilon_{con}} \tag{3}$$

$\dot{m}_p$ [kg/s]	D_t [cm]	D_e [cm]	D_c [cm]	L_c [cm]
0.279	1.15	19.86	3.63	11.43

Table 3: Preliminary DRY-1 geometry

The nozzle geometry was modelled with a conical convergent and a Rao parabolic divergent[6]. For the convergent a realistic cone angle of $\alpha_{con} = 30°$ was chosen from which its length can be computed.

$$L_{con} = \frac{D_c - D_t}{2\tan(\alpha_{con})} \tag{4}$$

Since no constraint was imposed on the divergent length a 100% bell percentage was selected in order to minimize 2D losses as described in section 4. From it, together with the area ratio, the parabolic nozzle can be defined. The nozzle's main characteristics are reported in Table 4

L_{con} [cm]	L_{div} [cm]	θ_e [deg]
2.15	34.91	4.329

Table 4: Nozzle main characteristics

A simplified geometrical model of the whole system is shown in Figure 2

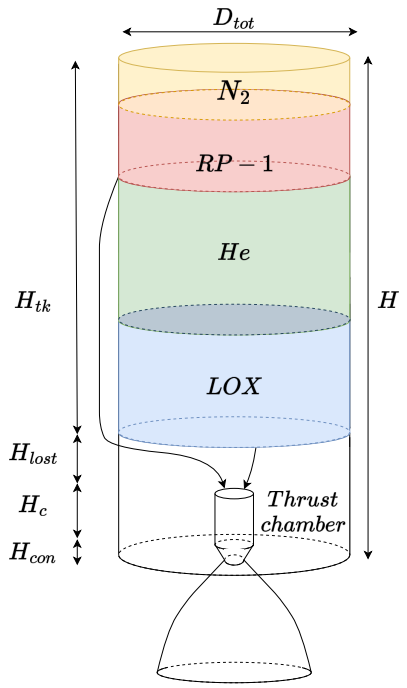

Figure 2: System configuration

A check on the compliance of the chamber Mach number is done ($M_c < 0.3$):

$$\frac{1}{\varepsilon_{con}} = M_c \left[\frac{1 + \frac{\gamma_c - 1}{2}}{1 + \frac{\gamma_c - 1}{2} M_c^2} \right]^{\frac{\gamma_c + 1}{2(\gamma_c - 1)}} \xrightarrow{fsolve} \quad M_c = 0.059 \tag{5}$$

From the geometry of the motor and the allocated space constraints, the total height of the tanks can be calculated. The volume around the thrust chamber (combustion chamber + convergent) can be assessed:

$$V_{tc} = \frac{\pi}{4} \left[L_c D_c^2 + \frac{L_{con}}{3} \left(D_c^2 + D_t^2 + D_c D_t \right) \right] \tag{6}$$

Also, the volume of the cylinder that covers the length of the thrust chamber and with the total diameter of 1 meter (D_{tot}) can be computed. From there, the empty volume around the thrust chamber can be computed as a difference:

$$V_{lost} = V_{tc} - \frac{\pi}{4} \left(L_c + L_{con} \right) D_{tot} \tag{7}$$

This value must be 20% of the total cylinder volume, as cited in subsection 2.1. As the computed value was lower, additional volume had to be removed from the tanks in order to meet the requirement. The height dedicated to the tanks is calculated as follow:

$$H_{tk} = H - \left[L_c + L_{con} + \frac{4}{\pi D_{tot}^2} \left(0.2 V_{tot} - V_{lost} \right) \right] \tag{8}$$

The total volume allocated to the tanks is hence fully defined. In order to calculate the masses of pressurizer and propellants, some assumption have to be made:

- adiabatic expansion of the pressurizing gas;
- blow-down ratios can be tuned;
- mean value of the oxidizer to fuel ratio.

A system of equations can be set up:

$$\begin{cases} \dfrac{m_{ox}}{m_{fu}} = \overline{O/F} \\ m_{ox} = \rho_{ox} V_{ox} \\ m_{fu} = \rho_{fu} V_{fu} \\ V_{ox} = V^{ox}_{pr,f} - V^{ox}_{pr,i} \\ V_{fu} = V^{fu}_{pr,f} - V^{fu}_{pr,i} \\ V^{ox}_{pr,f} = B_{ox}^{\frac{1}{\gamma_{pr,ox}}} V^{ox}_{pr,i} \\ V^{fu}_{pr,f} = B_{fu}^{\frac{1}{\gamma_{pr,fu}}} V^{fu}_{pr,i} \end{cases} \tag{9}$$

In order to solve System 9, the pressurizer and the initial temperature of the propellants have to be set. Different pressurizing gas are available, mainly nitrogen or helium are the most common choices. The main differences for the two are the storage temperature, the molar mass and the specific heat ratio. The latter parameter influences the adiabatic discharge, higher values implies faster pressure discharge. The molar mass affects the amount of gas to be embarked at a given pressure. The storage temperature is a matter of compatibility with the propellant. Nitrogen gas was chosen to pressurize RP-1 since no cryogenic conditions were present also it guarantees lower discharge, with the downside of increasing the mass of the system. On the other side, LOX required a cryogenic compatibility that can be ensured by helium. Even though an efficient insulating bladder is employed, the design choice was dictated by a more conservative approach: the employment of nitrogen also with LOX was discarded since storage temperature and pressure are not compatible with its properties[7].

T^{fu}_{pr} [K]	T^{ox}_{pr} [K]	γ_{N_2} [-]	γ_{He} [-]
300	90	1.40	1.67

Table 5: Initial values for pressurizer gases and specific heat ratio values

$\overline{O/F}$ [-]	$B_{pr,ox}$ [-]	$B_{pr,fu}$ [-]	V_{tot} [m^3]
2.42	2.5	2.5	1.27

Table 6: Assumed or calculated values as first iteration

The blowdown ratios B_{pr} are initially chosen assuming negligible losses and according to the boundaries imposed by the combustion chamber, as stated in subsection 2.1. This particular element deeply influences the whole dynamics and there were no reasons to set two different B_{pr}. The masses and volumes of oxidizer, fuel and pressurizing gases are than computed.

m_{fu} [kg]	m_{ox} [kg]	$V^{fu}_{pr,i}$ [m^3]	$V_{fu,i}$ [m^3]	$V^{ox}_{pr,i}$ [m^3]	$V_{ox,i}$ [m^3]
165.34	400.13	0.2217	0.2049	0.4789	0.3510

Table 7: Propellant and pressurizer quantities as first iteration

Finally, the feeding lines and the injectors plate of DRY-1 can be modelled. Considering Figure 2, the length of the pipes can be retrieved as a difference:

$$L_{fd}^{fu} = H - L_c - H_{tk,fu} \tag{10}$$

$$L_{fd}^{ox} = H - L_c - H_{tk} \tag{11}$$

The initial pressure drop across the injector Δp_{inj} has to be assumed as a percentage of the initial chamber pressure. An acceptable range of this fraction goes from 5% to 30%. A value of 20% is chosen for both oxidizer and fuel lines. The fuel and oxidizer injectors' area can be computed assuming reasonable values for the discharge coefficient C_d. A fair assumption has been made according to the superficial roughness quality of AM as explained in section 5.

$$\dot{m}_{fu} = \frac{1}{1+O/F}\dot{m}_p \qquad \dot{m}_{ox} = \frac{O/F}{1+O/F}\dot{m}_p \tag{12}$$

$$A_{inj}^{p} = \frac{\dot{m}_p}{C_d\sqrt{2\Delta p_{inj}\rho_p}} \tag{13}$$

Note that A_{inj}^{p} is referred or to fuel's injectors area or to oxidizer's injectors area calculated by the imposed conditions.
By assuming a diameter for the fuel injector (Table 1), the number of injectors can be computed:

$$A_{inj,single}^{fu} = \frac{\pi {D_{inj}^{fu}}^2}{4} \tag{14}$$

$$N_{inj}^{fu} = \left\lfloor \frac{A_{inj,fu}}{A_{inj,single\ fu}} \right\rfloor \tag{15}$$

For the injection plate, short tubes with conical entrance are assumed (see discussion in section 5) in a triplet configuration, matching as much as possible the predicted $\overline{O/F}$.

$$N_{inj}^{ox} = 2 \cdot N_{inj}^{fu} \tag{16}$$

The real A_{inj} will influence the diameters of the injectors, making them different from the supposed one. New values for the injectors diameters shall be calculated to respect the imposed A_{inj}. Final results are reported in Table 8.

N_{inj}^{fu} [−]	N_{inj}^{ox} [−]	D_{inj}^{fu} [mm]	D_{inj}^{fu} [mm]
3	6	1.12	1.13

Table 8: Propellant and pressurizer quantities as first iteration

Once the the geometry of the injection plate is established, feeding line losses were modelled. As shown in Equation 18, the dimension of the lines and the Darcy friction factor f are needed. This last coefficient depends on the Re and on the roughness and it is retrieved from Moody chart[8].
The speed of the fluid inside the lines is found from the mass flow rate and thus the losses along the whole system are computed via Equation 17, Equation 18, Equation 19. The diameter of the two feeding lines is assumed to be different to counter balance the effect of the different densities of the fluids.

D_{fd}^{fu} [mm]	D_{fd}^{ox} [mm]
5	7

Table 9: Diameter assumed for feeding lines

$$u_{p,fd} = \frac{\dot{m}_p}{A_{p,fd}\rho_p} \tag{17}$$

$$K_{p,tot} = 1 + f\frac{L_{p,fd}}{D_{p,fd}} + \left(\frac{A_{p,fd}}{A_{p,inj,tot}C_d}\right)^2 \tag{18}$$

$$\Delta p_p = \frac{1}{2}\rho_p k_{p,tot} u_{p,fd}^2 \tag{19}$$

Finally, the pressure inside the tanks can be computed. This value will influence the whole dynamics of the system and will be refined to maximize the total impulse.

$p_{fu,i}$ [bar]	$p_{ox,i}$ [bar]
60.79	60.19

Table 10: Initial tank pressure

As can be seen, values are similar between the two tanks despite the difference in fluid density, pipe length and pipe diameter, as the pressure cascade in a such compact system is mainly driven by the imposed pressure drop across the injectors, imposed to be equal.
Results of the nominal design will be presented in section 3.

2.3 System dynamics

From the nominal sizing of the engine, it is necessary to simulate the real dynamics of the system in order to:

- retrieve the performance of the designed system in time;
- check the compliance of the system with the constraints;
- test other designs through iteration to select the best one based on the simulated data of interest.

For this reasons, a numerical method was implemented. An high level explanation for the functioning of the algorithm can be appreciated in Figure 3.

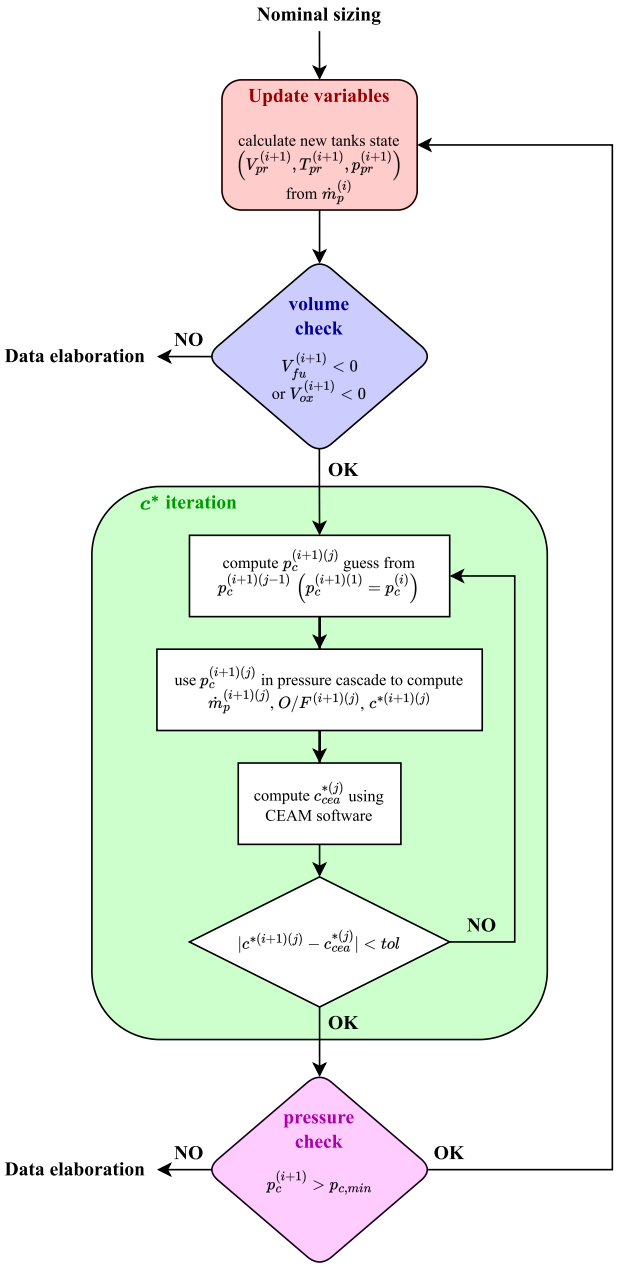

Figure 3: Flowchart of dynamics of the model

The first step of the time cycle is to update the state of the two tanks based on the previous iteration. Assuming a constant propellants flow rate during the time step Δt, the volume of the remaining liquid is decreased by a quantity $\Delta V^{(i+1)}$. Accordingly, the volume of the pressurizer will increase by the same amount.

$$\Delta V^{(i+1)} = \frac{\dot{m}_p^{(i)} \Delta t}{\rho_p} \tag{20}$$

$$V_p^{(i+1)} = V_p^{(i)} - \Delta V^{(i+1)} \tag{21}$$

$$V_{pr}^{(i+1)} = V_{pr}^{(i)} + \Delta V^{(i+1)} \tag{22}$$

From the change of volume, the new pressure and temperature of the pressurizer gas are computed assuming

an adiabatic expansion in the tank:

$$p_{pr}^{(i+1)} = p_{pr}^{(i)} \left(\frac{V_{pr}^{(i)}}{V_{pr}^{(i+1)}} \right)^{\gamma_{pr}} \tag{23}$$

$$T_{pr}^{(i+1)} = T_{pr}^{(i)} \left(\frac{V_{pr}^{(i)}}{V_{pr}^{(i+1)}} \right)^{\gamma_{pr}-1} \tag{24}$$

A check must be performed on the remaining volume of propellants in the tanks at current iteration: if the volume of fuel is negative it means that the combustion is over so the simulation stops (the same for oxidizer). If there is some more propellant to use, the iteration goes on with the calculation of the new chamber pressure. This step is complex because it introduces another cycle of iterations inside each time step. The mass flow rate of the propellants depends on the pressure cascade in the feeding lines, hence on the chamber pressure. These two variables are bounded and both unknown, but there's only one configuration that can match the boundary condition imposed by the critical condition in the throat, so the problem is well-posed.
From literature, the c^* of the chamber has the following expression:

$$c^* = \frac{p_c A_t}{\dot{m}_{fu} + \dot{m}_{ox}} \tag{25}$$

It correlates the chamber pressure with the propellants flow rate in the throat. Moreover, it only depends on the thermodynamics of the combustion process in the chamber, which changes over time due to the architecture of blow-down system. By imposing the critical conditions in the throat, it can be rewritten as:

$$c^* = \sqrt{\frac{\mathcal{R}}{\mathbb{M}} \frac{T_c}{\gamma} \left(\frac{\gamma+1}{2} \right)^{\frac{\gamma+1}{\gamma-1}}} \tag{26}$$

The system is coherent only if the two expressions give the same result. A system of equations could be created and numerically solved to match both the pressure cascade and c^*.
A reasonable initial guess for chamber pressure $p_c^{(i+1)(1)}$ is taken as the pressure at previous time step $p_c^{(i)}$. The next steps $p_c^{(i+1)(j)}$ will converge progressively towards the real current pressure $p_c^{(i+1)}$ (for increasing j).
From $p_c^{(i+1)(j)}$ the $c^{*(i+1)(j)}$ is computed from the pressure cascade as described in Equation 25:

$$u_{fd,p}^{(i+1)(j)} = \sqrt{\frac{2\left(p_{pr}^{(i+1)} - p_c^{(i+1)(j)}\right)}{\rho_p K_p}} \tag{27}$$

$$m_p^{(i+1)(j)} = \rho_p A_{fd,p} u_{fd,p}^{(i+1)(j)} \tag{28}$$

$$O/F^{(i+1)(j)} = \frac{m_{ox}^{(i+1)(j)}}{m_{fu}^{(i+1)(j)}} \tag{29}$$

$$c^{*(i+1)(j)} = \frac{A_t p_c^{(i+1)(j)}}{\dot{m}_{fu}^{(i+1)(j)} + \dot{m}_{ox}^{(i+1)(j)}} \tag{30}$$

Equation 26 is solved directly using CEAM software, which takes as input $p_c^{(i+1)(j)}$ and $O/F^{(i+1)(j)}$ to return $c_{cea}^{*(j)}$.
The two computed c^* are then compared: if their difference satisfies a certain tolerance, then the cycle stops and returns the new values for the current time step. Else, the inner cycle continues the refinement by guessing a new $p_c^{(i+1)(j+1)}$ from $p_c^{(i+1)(j)}$.
Finally, a check on the new combustion pressure $p_c^{(i+1)}$ is performed in order to stay above the minimum design pressure $p_{c,min}$, as mentioned in subsection 2.1. Similarly to the previous check, if the pressure drops below the limit the simulation stops and returns the results, else it continues with the next time step.

The same general algorithm is used to refine the initial assumptions of O/F and B, which influence the nominal design of the whole engine (as described in subsection 2.2). In this case, the initial c^* value from design

is assumed constant to reduce the computational burden, since the algorithm is applied over a wide range of combinations of O/F and B. This assumption is reasonable because the O/F (and as consequence the thermodynamics of the combustion) hardly varies during the whole burn, as can be noticed in **REFERENCE** .

3 Results analysis

4 Nozzle losses

In order to calculate and evaluate the nozzle losses, further modifications and calculations were added to the model previously presented in section 2. In particular 2D, throat erosion and boundary layer losses were considered.

4.1 Losses calculations

Each loss term has been calculated as follows:

- **2D losses**: for a parabolic Rao nozzle this loss can be computed in a similar way as a conical nozzle by applying Equation 31

$$\lambda = \frac{1}{2}\left[1 + \cos\left(\frac{\delta + \theta_e}{2}\right)\right] \tag{31}$$

  where δ is the cone angle of an fictitious conical nozzle with the same divergent length and area ratio[Sutton].

- **Throat erosion losses:** this effect is due to the increasing throat area over time whose behavior can be obtained by considering a constant erosion rate for simplicity. Since this loss is time dependent it needs to be considered inside the dynamic model of the system (subsection 2.3).

$$D_t^{(i+1)} = D_t^{(i)} + 2E_t\Delta t \tag{32}$$

  Usually the erosion rate is calculated through experimental measurements of the propulsion system, in this case a suitable erosion rate has been searched for in literature. Due to the smallness of the system, no acceptable rates were found, therefore, an increase of 2% of the initial throat radius over the entire burn was assumed.[Suttontesi_malesia]

- **Boundary layer losses:** to determine this contribution the effect of the boundary layer in the throat of the nozzle must be estimated. To achieve this the thermophysical properties of the exhaust gasses at the throat must be recovered from the CEAM outputs of the nominal design (subsection 2.2). From them the throat Reynolds number can be obtained.

$$Re_t = \frac{\rho_t D_t u_t}{\mu_t} \tag{33}$$

  Introducing the curvature of the throat, recovered from the Rao nozzle geometry, a modified Reynolds number is derived as follows:

$$k_t = 0.382\frac{D_t}{2} \tag{34}$$

$$Re' = \sqrt{\frac{D_t}{2k_t}}Re_t \tag{35}$$

  Now it is possible to calculate the throat discharge coefficient from which the real mass flow and effective throat area can be calculated.

$$C_{d,t} = 1 - \left(\frac{\gamma_t + 1}{2}\right)^{\frac{3}{4}}\left[3.266 - \frac{2.128}{\gamma_t + 1}\right]\frac{1}{\sqrt{Re'}} + 0.9428\frac{(\gamma_t - 1)(\gamma_t + 2)}{Re'\sqrt{\gamma_t + 1}} \tag{36}$$

$$\dot{m}_r = C_{d,t}\dot{m}_{id} \tag{37}$$

$$A_{t,eff} = \frac{\dot{m}_r c^*}{p_c} \tag{38}$$

4.2 Effects on the nominal design

Including all the losses in the dynamic model has a minor effect on the evolution of the throat area and discharge coefficient as can be seen both in Figure 4 and Figure 5. This is mainly due to the fact that the erosion rate was recovered by imposing a rather small variation of the throat area over time.

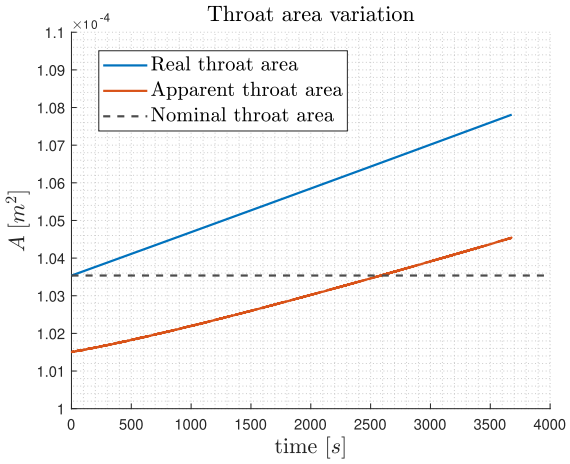

Figure 4: Throat area evolution

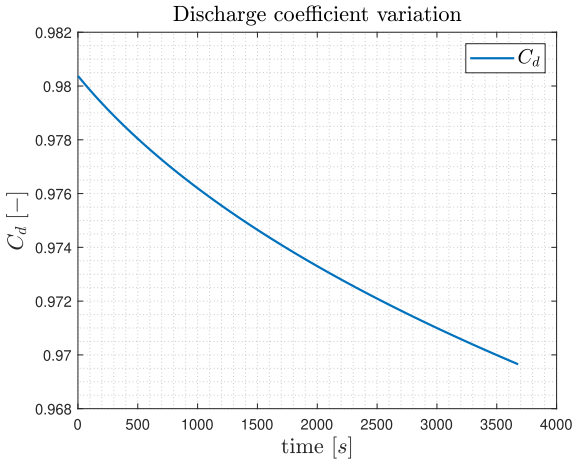

Figure 5: Throat discharge coefficient evolution

Where the real throat area describes its physical evolution due to erosion while the apparent one is the effective area as seen by the gas flow due also to the presence of the boundary layer. The throat area variation has repercussions over the entire system as the chamber pressure evolution is influenced, so are the pressure cascade, the propellants mass flow rate and all consequent physical quantities as can be seen in the following figures.

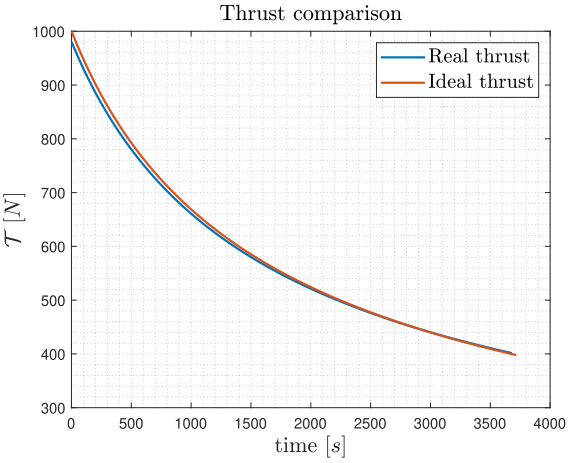

Figure 6: Thrust comparison

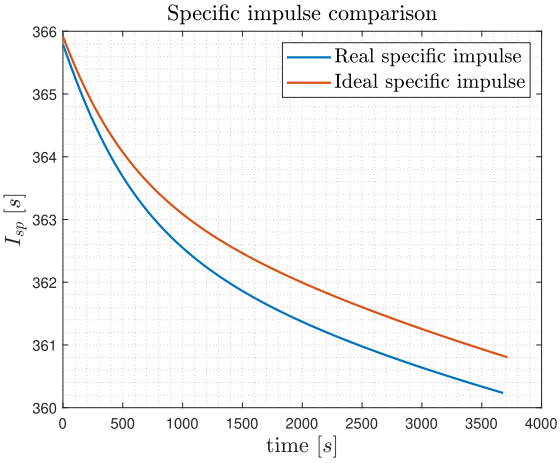

Figure 7: Specific impulse comparison

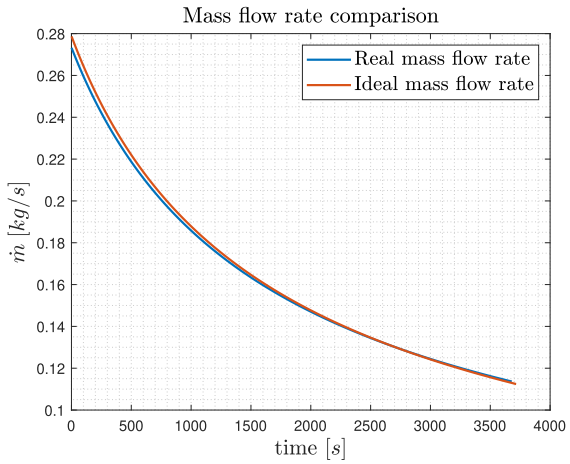

Figure 8: Propellants mass flow rate comparison

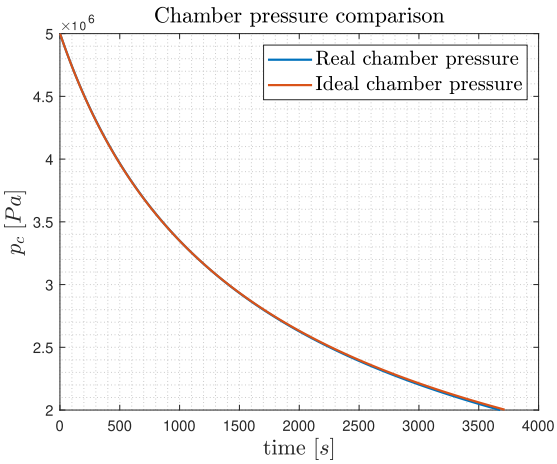

Figure 9: Combustion chamber pressure comparison

Again it is possible to appreciate the fairly small repercussions of these losses as all quantities exhibit basically the same behavior except the specific impulse, which tends to deviate more and more over time. This still holds true for the total impulse and the burn time as reported in Table 11.

	I_{tot} [N s]	t_b [s]
Ideal	$2.173 \cdot 10^6$	3716
Real	$2.140 \cdot 10^6$	3679

Table 11: Total impulse and burn time comparison

5 Additive manufacturing influences

6 Cooling analysis

Bibliography

[1] Robert-Jan Koopmans et Al. “Propellant Tank Pressurisation with Helium Filled Hollow Glass Microspheres”. In: (2015).

[2] H. C. Hearn. “Design and Development of a Large Bipropellant Slowdown Propulsion System”. In: (1995).

[3] G.P.Sutton. “Rocket Propulsion Elements”. In: (2017).

[4] Ariane Group. *Chemical bipropellant thruster family*. Site: https://www.space-propulsion.com/. 2021.

[5] Huzel and Huang. “Modern Engineering for design of Liquid-Propellant Rocket Engines”. In: (1992).

[6] G.V.Rao. “Exhaust Nozzle Contour for Optimum Thrust”. In: (1958).

[7] *NIST Chemistry WebBook*. URL: https://webbook.nist.gov/cgi/fluid.cgi?T=85&PLow=4&PHigh=5.5&PInc=0.1&Digits=5&ID=C7727379&Action=Load&Type=IsoTherm&TUnit=K&PUnit=bar&DUnit=mol%2Fl&HUnit=kJ%2Fkg&WUnit=m%2Fs&VisUnit=Pa*s&STUnit=N%2Fm&RefState=DEF. (accessed: 14.04.2024).

[8] Ajinkya A. More. “Analytical solutions for the Colebrook and White equation and for pressure drop in ideal gas flow in pipes”. In: (2005).